ATF4 Expression in Thermogenic Adipocytes is Required for Cold-Induced Thermogenesis in Mice via FGF21-Independent Mechanisms

Sarah H. Bjorkman[1,2*]; Alex Marti[1*]; Jayashree Jena[1]; Luis Miguel García-Peña[1]; Eric T. Weatherford[1]; Kevin Kato[1], Jivan Koneru[1], Jason H. Chen[1], Ayushi Sood[1], Matthew J. Potthoff[1,3]; Christopher M. Adams[1,4]; E. Dale Abel[1,5]; Renata O. Pereira[1]

[1]Fraternal Order of Eagles Diabetes Research Center and Division of Endocrinology and Metabolism, Roy J. and Lucille A. Carver College of Medicine, University of Iowa, Iowa City, IA, USA.

[2]Department of Obstetrics and Gynecology, Reproductive Endocrinology and Infertility, University of Iowa Hospital and Clinics, Iowa City, IA, USA

[3]Department of Neuroscience and Pharmacology, Roy J. and Lucille A. Carver College of Medicine, University of Iowa, Iowa City, IA, USA.

[4]Division of Endocrinology, Metabolism and Nutrition, Department of Medicine, Mayo Clinic, Rochester, Minnesota, USA.

[5]Department of Medicine, David Geffen School of Medicine, University of California, Los Angeles, Los Angeles, CA, USA

Lead contact:

e-mail: renata-pereira@uiowa.edu

Address: 169 Newton Road, 4338 PBDB | Iowa City, IA 52242

Phone: 319-335-9615

Fax: 319-335-386

*authors contributed equally to this work

Abstract:

In brown adipose tissue (BAT), short-term cold exposure induces the integrated stress response (ISR) main effector, activating transcription factor 4 (ATF4), and its downstream target fibroblast growth factor 21 (FGF21). We recently demonstrated that induction of ATF4 in BAT in response to mitochondrial stress is required for thermoregulation, at least in part, via induction of FGF21. In the present study, we tested the hypothesis that *Atf4* and *Fgf21* induction in BAT are both required for BAT thermogenesis by generating mice selectively lacking either *Atf4 (*ATF4 BKO*)* or *Fgf21* (FGF21 BKO) in UCP1-expressing adipocytes. After 3 days of cold exposure, core body temperature was significantly reduced in *ad-libitum*-fed ATF4 BKO mice, which correlated with *Fgf21* downregulation in brown and beige adipocytes, and impaired browning of white adipose tissue (WAT). Conversely, although *Fgf21* deletion in thermogenic adipocytes also reduced cold-induced browning of WAT, *ad libitum*-fed FGF21 BKO mice had preserved core body temperature after cold exposure. When cold-exposed under fasting conditions, both ATF4 BKO and FGF21 BKO mice had reduced cold tolerance. Mechanistically, ATF4 downregulation in thermogenic adipocytes decreased amino acid import and metabolism in BAT, likely contributing to impaired brown adipocyte thermogenic capacity under *ad libitum*-fed conditions. Thus, *Atf4* regulates *Fgf21* expression in thermogenic adipocytes during cold stress, which is required to mediate cold-induced browning of iWAT but is dispensable for thermoregulation in the fed state. In contrast, in the fasted state, both *Atf4* and *Fgf21* expression in thermogenic adipocytes are required for thermoregulation in mice.

Key words: ATF4 / FGF21 / Brown adipose tissue / amino acids metabolism / thermogenesis

Introduction:

Since the discovery of active brown adipose tissue (BAT) in adult humans, multiple studies have explored BAT thermogenic activation as a potential strategy for increasing energy expenditure and nutrient disposal to mitigate obesity and its complications (1, 2, 3). More recently, BAT has been recognized as a secretory organ, promoting the release of batokines that may act in an endocrine manner to regulate systemic metabolism (4). Indeed, several studies using β3-adrenergic agonists to activate BAT demonstrated changes in adiposity and improvements in glucose homeostasis (3, 5, 6), however, this class of medication poses cardiovascular concerns (1). Therefore, identifying new pathways that can be targeted to induce BAT's thermogenic activity and secretory function, may lead to the discovery of new targets to improve metabolic health.

A recent study demonstrated that the activating transcription factor 4 (ATF4), the main effector of the integrated stress response (ISR), is induced in brown adipocytes in response to cold exposure, which correlates with a significant increase in fibroblast growth factor 21 (FGF21) circulating levels (7). Furthermore, ATF4 overexpression in BAT is sufficient to improve thermogenesis in mice (8). Similarly, our recent work showed that selective deletion of the mitochondrial fusion protein optic atrophy 1 (OPA1) in BAT induces the expression and secretion of fibroblast growth factor 21 (FGF21) as a batokine, via an ATF4-dependent mechanism in mice. Activation of this ATF4-FGF21 axis was required to mediate an adaptive response characterized by elevated resting metabolic rates, and improved thermoregulation in OPA1-deficient mice (9). Together, these studies suggest that the ISR is likely to be operative in BAT under physiological circumstances and may regulate the secretion of FGF21 as a batokine. To date, studies investigating the functional significance of the ISR in BAT were performed in ATF4 whole-body knockout mice (10, 11, 12, 13, 14). Moreover, although FGF21 is induced in BAT in response to thermogenic activation, whether ATF4 is required for this induction, and whether BAT-derived FGF21 is necessary for adaptive thermogenesis was yet to be investigated.

In the present study, we investigated the requirement of ATF4 and FGF21 induction in thermogenic adipocytes for adaptive thermogenesis by generating mice with selective deletion of either *Atf4* or *Fgf21* in UCP1-expressing adipocytes. Our data demonstrated that neither ATF4 nor FGF21 are required for the activation of canonical thermogenic genes in BAT after 3 days of cold-exposure, however, *Atf4* expression in BAT was required for cold-induced upregulation of *Fgf21* and both *Atf4* and *Ffg21* expression were required for cold-induced browning of white adipose tissue (WAT). Nonetheless, core body temperature was significantly reduced in ATF4 BKO mice, but not in FGF21 BKO mice, when mice were cold exposed with free access to food. Noteworthy, in the absence food, both *Fgf21* and *Atf4* were required for thermoregulation in mice. Together, our study identified novel roles for ATF4 in BAT physiology in regulating core body temperature in a manner that is independent of *Fgf21* induction in thermogenic adipocytes or cold-induced browning. Our data points to an alternative mechanism downstream of *Atf4*, involving regulation of amino acids transport and metabolism to support cold-induced thermogenesis.

Study Design and Methods:

Mouse Models:

Experiments were performed in male and/or female mice on a C57Bl/6J background. $ATF4^{fl/fl}$ (15) and $FGF21^{fl/fl}$ mice (16) were generated as previously described. Transgenic mice expressing cre recombinase under the control of the *Ucp1* promoter (Tg (Ucp1-cre)1Evdr) (17) were acquired from the Jackson Laboratories (#024670), and were crossed with $ATF4^{fl/fl}$ and $FGF21^{fl/fl}$ mice to promote selective deletion of these genes in thermogenic adipocytes (ATF4 BKO and FGF21 BKO mice, respectively). $ATF4^{fl/fl}$ and $FGF21^{fl/fl}$ mice not expressing the Cre recombinase were used as wild type (WT) controls. Mice were weaned at 3 weeks of age and kept on standard chow (2029X Harlan Teklad, Indianapolis, IN, USA). Animals were housed at

22 °C with a 12-h light, 12-h dark cycle with free access to water and standard chow, unless otherwise noted. For cold exposure experiments, mice were acclimated to 30 °C (thermoneutral temperature for mice) for 7 days prior to being cold-exposed (4 °C). All mouse experiments presented in this study were conducted in accordance with animal research guidelines from the National Institutes of Health (NIH) and were approved by the University of Iowa Institutional Animal Care and Use Committee (IACUC).

Cold exposure experiments:

Core body temperature telemeters (Respironics, G2 E-Mitter, Murrysville, PA, USA) were surgically implanted into the abdominal cavity of 8-10-week-old mice. The mice were then allowed to recover for 6 days post-surgery, while individually housed in a rodent environmental chamber (Power Scientific, Pipersville, PA, USA) at 30 °C. Mice were then transferred to an OxyMax Comprehensive Lab Animal Monitoring System (CLAMS, Columbus Instruments International) at 30 °C for 3 days, followed by 4 °C for 3 days, as previously described (18). Core body temperature was recorded every 17 minutes throughout the experiment, along with O_2 and CO_2 levels, food intake, and ambulatory activity, as estimated by photoelectric beam breaks in the X + Y plane. Mice were fed *ad libitum* throughout the study. A separate cohort of mice underwent acute cold exposure following fasting. For these studies, 12-week-old mice were initially individually housed in the rodent environmental chamber at 30 °C for 7 days. At the end of the seventh day, mice were fasted for 12 hours (7 pm – 7 am). The initial temperature (t0) was recorded using a rectal probe (Fisher Scientific, Lenexa, KS, USA) at 7 am on day 8, after which the temperature was switched to 4 °C. Once the desired temperature was reached, we recorded rectal temperatures hourly for up to 4 hours of cold exposure. Mice remained without food throughout for the entirety of the experiment.

Glucose tolerance tests, nuclear magnetic resonance, and serum analysis

Glucose tolerance tests (GTT) and measurements of fasting glucose levels were performed as previously described (9). Serum FGF21 (BioVendor ELISA kit, Asheville, NC, USA) and GDF15 (R&D Systems, Minneapolis, MN, USA) were measured using commercially available kits according to the manufacturers' directions. Whole body composition was measured by nuclear magnetic resonance in the Bruker Minispec NF-50 instrument (Bruker, Billerica, MA, USA) (9).

Analysis of triglyceride levels

Triglycerides levels were measured in the liver of ATF4 BKO mice, using the EnzyChrom™ Triglyceride Assay Kit (BioAssay Systems, Hayward, CA, USA), as previously described (9).

RNA extraction and quantitative RT–PCR

Total RNA was extracted from tissues with TRIzol reagent (Invitrogen) and purified with the RNeasy kit (Qiagen Inc, Germantown, MD, USA). RNA concentration was determined by measuring the absorbance at 260 and 280 nm using a spectrophotometer (NanoDrop 1000, NanoDrop products, Wilmington, DE, USA). Total RNA (1 µg) was reverse-transcribed using the High-Capacity cDNA Reverse Transcription Kit (Applied Biosystems, Waltham, MA, USA), followed by qPCR reactions using SYBR Green (Life Technologies, Carlsbad, CA, USA) (19). Samples were loaded in a 384-well plate in triplicate, and real-time polymerase chain reaction was performed with an ABI Prism 7900HT instrument (Applied Biosystems, Waltham, MA, USA). The following cycle profile was used: 1 cycle at 95°C for 10 min; 40 cycles of 95°C for 15 s; 59°C for 15 s, 72°C for 30 s, and 78°C for 10 s; 1 cycle of 95°C for 15 s; 1 cycle of 60°C for 15 s; and 1 cycle of 95°C for 15 s. Data were normalized to *Gapdh* and *Tbp* expression and results are shown as relative mRNA levels. qPCR primers were designed using Primer-Blast or previously published sequences (20). Utilized primers are listed in Table 1.

Table 1. Primer sequences

Gene name	Forward	Reverse
Fgf21	TGACGACCAAGACACTGAAGC	TTTGAGCTCCAGGAGACTTTCTG
Atf4	AGCAAAACAAGACAGCAGCC	ACTCTCTTCTTCCCCCTTGC
Ucp1	GTGAAGGTCAGAATGCAAGC	AGGGCCCCCTTCATGAGGTC
Prdm16	CAGCACGGTGAAGCCATTC	GCGTGCATCCGCTTGTG
Gapdh	AACGACCCCTTCATTGAC	TCCACGACATACTCAGCAC
Dio2	AATTATGCCTCGGAGAAGACCG	GGCAGTTGCCTAGTGAAAGGT
Cpt1b	TGCCTTTACATCGTCTCCAA	AGACCCCGTAGCCATCATC
Evlov6	TCAGCAAAGCACCCGAAC	AGCGACCATGTCTTTGTAGGAG
Ppargc1α	GTAAATCTGCGGGATGATGG	AGCAGGGTCAAAATCGTCTG
Gdf15	GAGAGGACTCGAACTCAGAAC	GACCCCAATCTCACCTCTG
Slc7a1	CGT GAG TAC GCG ATC CTT GT	AGG ACC AAG ATG GAC TCG GA
Slc1a4	GTG GCA TCG CTG TTG CTT AC	GAC GTA GTG AAT GCG GCA AC
Slc7a11	GTC TGC CTG TGG AGT ACT GT	ATT ACG AGC AGT TCC ACC CA
Slc7a5	ATC GTA GGT CCT GCC ATG TG	ACC GTG TCT GAG CTA GTT GC
Asns	TAC AAC CAC AAG GCG CTA CA	AAG GGC CTG ACT CCA TAG GT
Tbp	ACC CTT CAC CAA TGA CTC CTA TG	TGA CTG CAG CAA ATC GCT TGG

RNA Sequencing

RNA sequencing was performed in BAT of male ATF4 BAT KO mice cold exposed for 3 days by the Iowa Institute of Human Genetics: Genomics Division at the University of Iowa. Sequencing libraries were prepared using the Illumina TruSeq mRNA Stranded kit and sequenced on a HiSeq4000. Two approaches were used for read alignment, mapping, and quantification. First,

a workflow using HISAT2 (v2.1.0), featureCounts (v1.6.3), and DESeq2 (v1.22.2) was performed (21, 22, 23). The second approach used pseudo-alignment and quantification with Kallisto (v0.45.0) and DESeq2 for differential expression analysis (24). Ingenuity® Pathway Analysis (IPA®) software from Qiagen was utilized for identification of potentially modified pathways. Data visualization was performed using pheatmap and ggplot2 packages in R. RNA-seq data have been deposited to the GEO database.

Western blot analysis

Immunoblotting analysis was performed as previously described (25). Approximately, 50 mg of frozen tissue was homogenized in 200 µl lysis buffer containing (in mmol/l) 50 HEPES, 150 NaCl, 10% glycerol, 1% Triton X-100, 1.5 $MgCl_2$, 1 EGTA, 10 sodium pyrophosphate, 100 sodium fluoride, and 100 µmol/l sodium vanadate. Right before use, HALT protease/phosphatase inhibitors (Thermo Fisher Scientific, Waltham, MA, USA) were added to the lysis buffer and samples were processed using the TissueLyser II (Qiagen Inc., Germantown, MD, USA). Tissue lysates were resolved on SDS–PAGE and transferred to nitrocellulose membranes (Millipore Corp., Billerica, MA, USA). Membranes were incubated with primary antibodies overnight at 4 °C and with secondary antibodies for 1 h, at room temperature.

Antibodies

Primary Antibodies: GAPDH (1:1,000, Cell Signaling Technology, Danvers, MA, USA, #2118), UCP1 (1:1,000, Abcam, Boston, MA, USA, #Ab10983), phosphorylated eIF2α serine 51 (1:1,000, Cell Signaling Technology, #3597), total eIF2α (1:500, Santa Cruz Biotechnology, Dallas, TX, USA, #SC81261), phosphorylated S6 (1:1,000, Cell Signaling Technology, #4858), total S6 (1:1,000, Cell Signaling Technology, #2317) and β-actin (1:1,000, Sigma Aldrich, St.

Louis, MO, USA, # A2066). Secondary antibodies: IRDye 800CW anti-mouse (1:10,000, LI-COR, Lincoln, NE, USA, #925-32212) and Alexa Fluor anti-rabbit 680 (1:10,000, ThermoFisher Scientific, #A27042). Fluorescence was quantified using the LiCor Odyssey imager.

Data analysis

Unless otherwise noted, all data are reported as mean ± SEM. Student's *t*-test was performed for comparison of two groups. A probability value of $P \leq 0.05$ was considered significantly different. Statistical calculations were performed using the GraphPad Prism software (La Jolla, CA, USA). The CalR software was used to extract the averaged data for the metabolic parameters measured in the CLAMS at 30 °C and 4 °C for both, the light and dark cycles. The hourly plots for body temperature were also extracted from CalR (26).

Results:

The Integrated stress response is induced in BAT after 3 days of cold exposure

The ISR was shown to be potently induced in BAT in response to acute cold-stress (4-6 hours) following a 12-hour fast, which correlated with high serum levels of FGF21 and growth differentiation factor 15 (GDF15), downstream targets of the ISR (7). We, therefore, first sought to examine if this pathway was also induced after 3 days of cold exposure in *ad libitum*-fed conditions. Mice were acclimated to thermoneutrality (30 °C) for 7 days, after which they were exposed to 4 °C for 3 days. Our data demonstrated increased eIF2α phosphorylation (Figure 1A), and induction of *Atf4*, *Fgf21* and *Gdf15* mRNA levels in BAT (Figure 1B) in response to 3-days of cold exposure, confirming activation of the ISR. To investigate whether ISR activation in BAT is required for adaptive thermogenesis, we generated mice lacking the main effector of the ISR, ATF4, selectively in BAT (ATF4 BKO mice). *Atf4* expression was significantly decreased in BAT of KO mice (Figure 1C), while it was preserved in the inguinal white adipose tissue (iWAT)

(Figure 1D) at ambient temperature conditions. *Fgf21* and *Gdf15* mRNA (Figure 1E) expression in BAT and their respective circulating levels (Figure 1F and G) were unchanged between WT and KO mice at baseline conditions.

ATF4 BAT KO Mice Have Reduced BAT Mass and Modestly Impaired Glucose Tolerance at Baseline Conditions

Because global ATF4 deletion has been associated with changes in systemic metabolism (12, 13), we evaluated body composition, energy metabolism, and glucose homeostasis in 8-week-old ATF4 BKO mice. Body mass (Fig. 2A), total fat mass (Fig. 2B) and total lean mass (Fig. 2C) were unchanged between KO mice and their WT littermate controls. The weight of inguinal (Fig. 2D) and gonadal (Fig. 2E) white adipose tissues (iWAT and gWAT, respectively) were unchanged between genotypes, while brown adipose tissue (BAT) mass was significantly reduced in ATF4 BKO mice (Fig. 2F). Interestingly, UCP1 protein levels were significantly reduced in BAT of ATF4 BKO mice at baseline conditions (Fig. 2G), while core body temperature was unchanged (Supplemental Fig. 1A). Likewise, food intake (Fig. 2H), locomotor activity (Fig. 2I), and energy expenditure (Fig. 2J) were unaffected by *Atf4* deletion. To assess the impact of *Atf4* deletion in thermogenic adipocytes on glucose homeostasis, we performed glucose tolerance tests (GTT). ATF4 BKO mice had a modest impairment in glucose clearance (Fig. 2K), as demonstrated by increased area under the curve for the GTT (Fig. 2L), and higher fasting glucose levels after a 6-hour fast (Fig. 2M), while liver triglyceride levels were comparable between genotypes (Fig. 2N).

ATF4 expression in BAT is required for thermoregulation in mice

To determine the requirement of ATF4 expression in BAT for adaptive thermogenesis, we monitored core body temperature in ATF4 BKO mice and their WT littermate controls during 3 days of cold exposure (4 °C). Core body temperature was significantly reduced in KO mice

during cold exposure (Fig. 3A and B). Despite having reduced thermoregulatory capacity, the metabolic phenotype of ATF4 BKO mice was largely unaffected, with no significant changes in energy expenditure (Supplemental Fig. 1B), locomotor activity (Supplemental Fig. 1C), and food intake (Supplemental Fig. 1D) during cold exposure, when compared to WT littermate controls. Cold-induced mRNA expression of *Fgf21* (Fig. 3C) was significantly reduced in ATF4 BKO mice, but serum levels were unaffected by ATF4 deficiency in BAT (Fig. 3D). Reduced core body temperature correlated with a significant decrease in BAT mass (Fig. 3E), however, relative mRNA expression of thermogenic genes was unchanged between genotypes (Fig. 3F). UCP1 protein levels (Fig. 3G) were also modestly, but significantly, decreased in BAT of KO mice after cold exposure. Browning of WAT is induced in response to 3 days of cold exposure and is believed to contribute to thermoregulation in mice (18). We, therefore, assessed browning of inguinal WAT (iWAT) in WT and ATF4 BKO mice. *Atf4* mRNA expression was significantly reduced in iWAT of KO mice after cold exposure (Fig. 3H). Moreover, activation of the thermogenic gene program was attenuated (Fig. 3I), and UCP1 protein levels were significantly reduced in in iWAT of KO mice (Fig. 3J), suggesting impaired cold-induced browning.

An earlier study reporting potent activation of ATF4 in BAT in response to acute cold exposure was performed following fasting, which correlated with an exacerbated induction in FGF21 serum levels (7). To test the role of ATF4 in thermoregulation and in FGF21 induction in BAT under these conditions, a separate cohort of ATF4 BKO mice was cold-exposed for 4 hours following a 12-hour fast. Core body temperature was significantly reduced in ATF4 BKO relative to their WT counterparts (Fig. 3K). Interestingly, in response to acute cold exposure, ATF4 was not required to regulate *Fgf21* mRNA expression in BAT (Fig. 3L) or FGF21 serum levels (Fig. 3M). Surprisingly, a subset of thermogenic genes was significantly induced in BAT of ATF4 BKO mice (Fig. 3N), while UCP1 protein levels were unchanged between ATF4 BKO mice and WT

control (Fig. 3O). Furthermore, activation of thermogenic genes in iWAT was similar between WT and ATF4 BKO mice (Fig. 3P).

FGF21 BAT KO Mice Have Normal Body Weight and Glucose Homeostasis at Baseline Conditions

To test the role of *Fgf21* expression in thermogenic adipocytes, we selectively deleted *Fgf21* in *Ucp1*-expressing adipocytes (FGF21 BKO). Because global FGF21 deletion was reported to cause changes in glucose and energy homeostasis (16, 27), we evaluated body composition, energy metabolism, and glucose homeostasis in 8-week-old FGF21 BKO mice fed chow diet. Body mass (Fig. 4A), total fat mass (Fig. 4B) and total lean mass (Fig. 4C) were unchanged between KO mice and their WT littermate controls. Food intake (Fig. 4D), locomotor activity (Fig. 4E) and energy expenditure (Fig. 4F) were also not significantly different between genotypes. To assess the impact of FGF21 deletion in thermogenic adipocytes on glucose homeostasis, we performed glucose tolerance tests (GTT). FGF21 BKO mice had similar systemic glucose homeostasis as WT mice, as demonstrated by unchanged areas under the curve for the GTT (Fig. 4G and H), and fasting glucose levels after a 6-hour fast (Fig. 4I).

FGF21 Expression in Thermogenic Adipocyte Is Dispensable for Thermoregulation

Because *Fgf21* mRNA expression was significantly reduced in ATF4 BKO mice after cold exposure, we directly tested the role of FGF21 in thermogenesis by exposing FGF21 BKO mice to cold stress. Core body temperature, as measured by telemetry, was unchanged between WT and FGF21 BKO mice at thermoneutrality (Supplemental Fig. 2A) and during 3 days of cold exposure (Fig. 5A and B). Although *Fgf21* mRNA levels were significantly reduced in BAT (Fig. 5C), FGF21 serum levels (Fig. 5D) were unchanged between genotypes. BAT mass normalized to body weight was unaffected by FGF21 deletion (Fig. 5E). Likewise, cold-induced activation of thermogenic genes was preserved (Fig. 5F), and UCP1 protein levels were similar in BAT of WT

and FGF21 BKO mice (Fig. 5G). Next, we evaluated the effects of FGF21 deletion on WAT browning. *Fgf21* mRNA levels were significantly reduced in the inguinal white adipose tissue (iWAT) of cold-exposed FGF21 BKO mice (Fig. 5H), which correlated with reduced mRNA levels of the thermogenic genes *Ucp1* and *Ppargc1α* (Fig. 5I), and with significantly lower UCP1 protein levels (Fig. 5J). Metabolically, energy expenditure (Supplemental Fig. 2B), food intake (Supplemental Fig. 2C) and locomotor activity (Supplemental Fig. 2D) were unchanged in FGF21 BKO mice during cold exposure. In contrast, in response to acute cold exposure following fasting, FGF21 BKO mice had reduced tolerance to cold relative to their WT counterparts (Fig. 5K). Although *Fgf21* mRNA levels were significantly reduced in BAT (Fig. 5L), FGF21 serum levels (Fig. 5M), thermogenic gene expression (Fig. 5N) and UCP1 protein levels (Fig. 5O) were similar in BAT between genotypes. Interestingly, cold-induced activation of thermogenic genes in iWAT was also reduced in FGF21 BKO mice under fasting conditions (Fig. 5P). Together, our data reinforce a role for FGF21 on cold-induced browning of WAT and suggest that impaired browning in the absence of defective BAT thermogenesis is insufficient to hamper thermoregulation in mice. Our data also indicate that defective *Fgf21* expression in ATF4 BKO mice is unlikely to impair thermoregulation in these mice. Finally, our data suggest that FGF21 induction in BAT does not contribute to FGF21 serum levels in response to cold exposure, is dispensable for cold-induced thermogenesis in *ad libitum*-fed conditions, but is required for thermoregulation in response to acute exposure under fasting conditions.

Transcriptome Analysis Reveals Downregulation of Genes Involved in Amino Acids Metabolism in ATF4 BKO Mice

To gain insight into the molecular mechanisms driving impaired thermoregulation in ATF4 BKO mice, we performed RNA sequencing (RNASeq) in BAT collected from 10-12-week-old mice lacking ATF4 in thermogenic adipocytes (ATF4 BAT KO) and their respective wild-type (WT) littermate controls after 3 days of cold exposure. In addition to confirming downregulation of

Fgf21 in ATF4 BKO mice, our transcriptome data revealed that several amino acids transporters were amongst the top downregulated genes in ATF4-deficient BAT (Fig. 6A). Furthermore, Ingenuity Pathway Analysis uncovered that genes involved in amino acids synthesis and metabolism were repressed in cold-exposed ATF4 BKO mice relative to their WT counterparts (Fig. 6B). Repression of amino acids metabolism-related genes in ATF4 BKO mice after 3 days of cold exposure was confirmed by qPCR (Fig. 6C); Meanwhile, these genes were unchanged in BAT of cold-exposed FGF21 BAT KO mice under the same conditions (Supplemental Fig. 3A) or in ATF4 BKO mice subjected to 4 hours of cold exposure following fasting (Supplemental Fig. 3B). Furthermore, mTOR signaling pathway, as measured by phosphorylated ribosomal protein S6, was reduced in BAT of cold-exposed ATF4 BKO mice relative to WT controls (Figure 6D). Together, these data suggest that ATF4, but not FGF21 is required to regulate amino acid import and metabolism into BAT during cold exposure and may also regulate mTOR signaling in response to cold, thereby contributing to thermogenic regulation in mice. Interestingly, under fasting conditions, ATF4 is dispensable to regulate amino acid transporters in BAT.

Discussion:

ATF4 was recently shown to be potently induced in BAT in response to acute cold exposure, which correlated with increased FGF21 serum levels (7). However, studies have shown that mice with global deletion of the *Atf4* gene have increased energy expenditure and induced *Ucp1* expression in BAT (13). Furthermore, these mice are better able to maintain core body temperature during a 7-h cold challenge (14). Nonetheless, a recent study demonstrated that adult-onset conditional *Atf4* deletion in agouti-related peptide neurons in the hypothalamus of mice is sufficient to increase energy expenditure, and enhance thermogenesis in BAT, suggesting that this phenotype is likely centrally regulated, rather than a result of *Atf4* deficiency in BAT (28). Indeed, our recently published study demonstrated that deletion of the

mitochondrial protein optic atrophy 1 (OPA1) in BAT lead to upregulation of *Atf4*, which was required for the induction and secretion of FGF21 as a batokine and was associated with improved thermoregulation (9). Moreover, a recent study showed that selective induction of ATF4 in brown adipocytes improves cold tolerance in mice (8). Here, we tested the requirement of ATF4 and FGF21 expression in thermogenic adipocytes for cold-induced thermogenesis. We demonstrated that neither ATF4 nor FGF21 are required for the activation of canonical thermogenic genes in BAT after cold-exposure. However, core body temperature was significantly reduced in ATF4 BKO mice, but not in FGF21 BKO mice, when mice were cold exposed with free access to food. Together, our study identified novel roles for ATF4 in BAT physiology in regulating core body temperature in a manner that seems to be independent of *Fgf21* induction, but may require ATF4-mediated regulation of amino acids import and metabolism to support cold-induced thermogenesis.

Thermogenic stimulation has been shown to strongly induce *Fgf21* expression in BAT via mechanisms that involve canonical activation of β-adrenergic signaling pathways (18). However, in our recent study, we demonstrated that FGF21 can be induced even when BAT's thermogenic function is dampened, via ATF4 activation (9). ATF4 has been shown to bind to the FGF21 promoter and to induce its transcription in several models (29, 30, 31). Nonetheless, whether ATF4 is required for cold-induced upregulation of FGF21 in BAT remained to be elucidated. In the present study, we show that mice lacking ATF4 specifically in thermogenic adipocytes (ATF4 BKO) have reduced core body temperature after 3 days of cold exposure in the absence of major changes in the expression of thermogenic genes in BAT. Additionally, energy expenditure was unchanged in these animals at thermoneutrality and during cold exposure. Although thermogenic gene activation was maintained in BAT, cold-induced *Fgf21* mRNA expression was reduced in thermogenic adipocytes (BAT and iWAT), and cold-induced browning of WAT was attenuated in ATF4 BKO mice. Therefore, next we directly tested whether

FGF21 is required to promote cold-induced thermogenesis, by generating mice lacking FGF21 selectively in thermogenic adipocytes.

Cold exposure is known to stimulate FGF21 expression in both humans and animal models; however, the source of circulating FGF21 and its metabolic consequences for adaptive thermogenesis are still incompletely understood (32, 33). A study in FGF21 global KO mice showed that ablation of FGF21 leads to an impaired response to cold stress when placing mice from 27° C to 5° C for 3 days (18). In UCP1 knockout (KO) mice, BAT was suggested as a potential source of circulating FGF21 upon long-term cold exposure, which was associated with increased browning of subcutaneous WAT relative to WT mice. However, a study in UCP1-FGF21 double knockout mice demonstrated that FGF21 is dispensable for this phenotype, as well as for the changes in energy expenditure and thermoregulation during prolonged cold exposure (34). Furthermore, a recent study demonstrated that liver-derived, but not adipose-derived FGF21 is required to maintain core body temperature in the first few hours of cold exposure (35). Therefore, although FGF21 may be dispensable for the adaptation to gradual long-term cold exposure in UCP1 KO mice, liver-derived FGF21 is required for thermoregulation in more acute scenarios. Regarding the source of FGF21, our data in ATF4 BKO mice, in which cold-induced FGF21 expression is diminished in BAT and WAT, could suggest that FGF21 expression in thermogenic adipocytes might be necessary for the regulation of core body temperature in response to short-term cold exposure in mice. However, our data in FGF21 BKO mice revealed no changes in BAT thermogenic activation or core body temperature after 3 days of cold exposure, even though cold-induced browning of WAT was attenuated. These data reinforce a role for FGF21 on cold-induced browning of WAT, as previously reported (18, 36, 37), and suggest that impaired browning is insufficient to hamper effective thermoregulation in mice when BAT thermogenesis is preserved. Our data also indicate that defective *Fgf21* expression in ATF4 BKO mice is unlikely to play a role on the impaired thermoregulatory capacity observed in these mice.

Transcriptome data in BAT of cold-exposed ATF4 BKO mice revealed that, in addition to reduced *Fgf21* transcript levels, gene expression of several amino acid transporters and amino acid metabolism genes was repressed relative to WT control mice. A recent study showed that cold stimuli potently increase mitochondrial brain chain amino acids (BCAA) uptake and oxidation in BAT, leading to enhanced BCAA clearance in the circulation. Furthermore, defective BCAA catabolism in BAT leads to impaired BCAA clearance and reduced thermogenesis in mice (38), suggesting that BCAA catabolism in BAT is required for proper thermoregulation. Furthermore, over the last several years, the mechanistic target of rapamycin (mTOR) signaling pathway has been reported to affect BAT function in rodents. Studies from independent groups showed that mTORC1 activity is highly induced by acute and chronic cold exposure and β3-adrenergic receptor stimulation (39, 40, 41). Furthermore, loss of mTORC1 in adipocytes reduces BAT size and completely prevents cold-induced BAT expansion, mitochondrial biogenesis, and oxidative metabolism in mice (40, 41, 42). Here, we show that phosphorylation of the downstream mTORC1 target ribosomal protein 6 (S6) is reduced in ATF4-deficient BAT after 3 days of cold exposure, suggesting that ATF4 induction in response to cold may regulate mTORC1 pathway to promote thermogenesis in BAT. Indeed, a recent study showed that ATF4 overexpression in BAT improves cold-induced thermogenesis, which seems to be dependent on increased S6 phosphorylation, and is attenuated upon treatment with the mTOR inhibitor rapamycin (8).

Of note, in the present study we reveal a novel role for FGF21 expression in thermogenic adipocytes in the modulation of core body temperature under fasting conditions. Although FGF21 BKO mice showed no change in core body temperature when cold exposed under *ad libitum*-fed conditions, acute cold exposure following an overnight fast reduced core body temperature in FGF21 BKO mice to a similar degree as observed in ATF4 BKO mice. Furthermore, although browning of iWAT was unaffected in ATF4 BKO mice, FGF21 BKO had

reduced expression of thermogenic genes in iWAT, suggesting attenuated browning. Although additional studies are needed to clarify the molecular mechanisms underlying these changes in core body temperature, here we show that they occur independently of changes in UCP1 protein levels or amino acid transport regulation in BAT of ATF4 BKO or FGF21 BKO mice.

In conclusion, by using mouse models of selective deletion of *Atf4* and *Fgf21* in thermogenic adipocytes, our study unraveled new roles for ATF4 and FGF21 for thermoregulation in mice. Together, our data demonstrated that *Atf4* deletion in thermogenic adipocytes impairs thermoregulation in mice, in a manner that seems independent of ATF4-mediated *Fgf21* expression or browning of WAT. Rather, ATF4 BKO mice had reduced expression of amino acid transporter genes and impaired mTOR signaling, suggesting ATF4 might contribute to BAT thermogenesis by increasing amino acid metabolism and by activating mTOR signaling in response to cold exposure. In contrast, FGF21 BKO mice had preserved thermoregulation, and normal cold-induced activation of thermogenesis genes in BAT, despite having reduced browning of WAT. Importantly, in the absence of food, both ATF4 and FGF21 are required to maintain core body temperature in mice in a manner that is independent of changes in UCP1 levels.

Acknowledgment

This work was supported by grants HL127764 and HL112413 from the NIH, 20SFRN35120123 from the American Heart Association (AHA) and the Teresa Benoit Diabetes research fund to E.D.A., who is an established investigator of the AHA; by NIH DK125405 to R.O.P.; by the Diabetes Research Training Program funded by the NIH (T32DK112751-01) to S.H.B and to J.J.; and by the NIH 1R25GM116686 to L.M.G.P. Metabolic phenotyping was performed at the Metabolic Phenotyping Core at the Fraternal Order of Eagles Diabetes Research Center. Analysis of mRNA expression was performed by qPCR at the Genomics Division at The Iowa Institute of Human Genetics.

Author Contributions:

S.H.B. and A.M. designed and conducted the experiments, analyzed data and helped write the manuscript. E.T.W., L.M.G.P, J.J. and K.K., conducted experiments and analyzed data. K.K., J.K., J.C. and A.S. aided with animal work and processed tissues for biochemical analysis. M.J.P., C.A. and E.D.A. provided essential materials and critical expertise. R.O.P. conceived the project, coordinated all aspects of this work, and assisted with manuscript writing and editing. E.D.A. assisted with manuscript editing.

Competing Interests:

The authors declare no competing interests.

References:

1. Cypess AM, Weiner LS, Roberts-Toler C, Franquet Elia E, Kessler SH, Kahn PA, et al. Activation of human brown adipose tissue by a beta3-adrenergic receptor agonist. Cell Metab. 2015;21(1):33-8.

2. Ruiz JR, Martinez-Tellez B, Sanchez-Delgado G, Osuna-Prieto FJ, Rensen PCN, Boon MR. Role of Human Brown Fat in Obesity, Metabolism and Cardiovascular Disease: Strategies to Turn Up the Heat. Prog Cardiovasc Dis. 2018;61(2):232-45.

3. Finlin BS, Memetimin H, Zhu B, Confides AL, Vekaria HJ, El Khouli RH, et al. The beta3-adrenergic receptor agonist mirabegron improves glucose homeostasis in obese humans. J Clin Invest. 2020;130(5):2319-31.

4. Villarroya J, Cereijo R, Gavalda-Navarro A, Peyrou M, Giralt M, Villarroya F. New insights into the secretory functions of brown adipose tissue. J Endocrinol. 2019;243(2):R19-R27.

5. O'Mara AE, Johnson JW, Linderman JD, Brychta RJ, McGehee S, Fletcher LA, et al. Chronic mirabegron treatment increases human brown fat, HDL cholesterol, and insulin sensitivity. J Clin Invest. 2020;130(5):2209-19.

6. Cero C, Lea HJ, Zhu KY, Shamsi F, Tseng YH, Cypess AM. beta3-Adrenergic receptors regulate human brown/beige adipocyte lipolysis and thermogenesis. JCI Insight. 2021;6(11).

7. Flicker D, Sancak Y, Mick E, Goldberger O, Mootha VK. Exploring the In Vivo Role of the Mitochondrial Calcium Uniporter in Brown Fat Bioenergetics. Cell Rep. 2019;27(5):1364-75 e5.

8. Paulo E, Zhang Y, Masand R, Huynh TL, Seo Y, Swaney DL, et al. Brown adipocyte ATF4 activation improves thermoregulation and systemic metabolism. Cell Rep. 2021;36(12):109742.

9. Pereira RO, Marti A, Olvera AC, Tadinada SM, Bjorkman SH, Weatherford ET, et al. OPA1 deletion in brown adipose tissue improves thermoregulation and systemic metabolism via FGF21. Elife. 2021;10.

10. Bettaieb A, Matsuo K, Matsuo I, Wang S, Melhem R, Koromilas AE, et al. Protein tyrosine phosphatase 1B deficiency potentiates PERK/eIF2alpha signaling in brown adipocytes. PLoS One. 2012;7(4):e34412.

11. Liu Z, Gu H, Gan L, Xu Y, Feng F, Saeed M, et al. Reducing Smad3/ATF4 was essential for Sirt1 inhibiting ER stress-induced apoptosis in mice brown adipose tissue. Oncotarget. 2017;8(6):9267-79.

12. Seo J, Fortuno ES, 3rd, Suh JM, Stenesen D, Tang W, Parks EJ, et al. Atf4 regulates obesity, glucose homeostasis, and energy expenditure. Diabetes. 2009;58(11):2565-73.

13. Wang C, Huang Z, Du Y, Cheng Y, Chen S, Guo F. ATF4 regulates lipid metabolism and thermogenesis. Cell Res. 2010;20(2):174-84.

14. Wang C, Xia T, Du Y, Meng Q, Li H, Liu B, et al. Effects of ATF4 on PGC1alpha expression in brown adipose tissue and metabolic responses to cold stress. Metabolism. 2013;62(2):282-9.

15. Ebert SM, Dyle MC, Kunkel SD, Bullard SA, Bongers KS, Fox DK, et al. Stress-induced skeletal muscle Gadd45a expression reprograms myonuclei and causes muscle atrophy. J Biol Chem. 2012;287(33):27290-301.

16. Potthoff MJ, Inagaki T, Satapati S, Ding X, He T, Goetz R, et al. FGF21 induces PGC-1alpha and regulates carbohydrate and fatty acid metabolism during the adaptive starvation response. Proc Natl Acad Sci U S A. 2009;106(26):10853-8.

17. Kong X, Banks A, Liu T, Kazak L, Rao RR, Cohen P, et al. IRF4 is a key thermogenic transcriptional partner of PGC-1alpha. Cell. 2014;158(1):69-83.

18. Fisher FM, Kleiner S, Douris N, Fox EC, Mepani RJ, Verdeguer F, et al. FGF21 regulates PGC-1alpha and browning of white adipose tissues in adaptive thermogenesis. Genes Dev. 2012;26(3):271-81.

19. Pereira RO, Tadinada SM, Zasadny FM, Oliveira KJ, Pires KMP, Olvera A, et al. OPA1 deficiency promotes secretion of FGF21 from muscle that prevents obesity and insulin resistance. EMBO J. 2017;36(14):2126-45.

20. Kim KH, Jeong YT, Oh H, Kim SH, Cho JM, Kim YN, et al. Autophagy deficiency leads to protection from obesity and insulin resistance by inducing Fgf21 as a mitokine. Nat Med. 2013;19(1):83-92.

21. Kim D, Paggi JM, Park C, Bennett C, Salzberg SL. Graph-based genome alignment and genotyping with HISAT2 and HISAT-genotype. Nat Biotechnol. 2019;37(8):907-15.

22. Liao Y, Smyth GK, Shi W. featureCounts: an efficient general purpose program for assigning sequence reads to genomic features. Bioinformatics. 2014;30(7):923-30.

23. Love MI, Huber W, Anders S. Moderated estimation of fold change and dispersion for RNA-seq data with DESeq2. Genome Biol. 2014;15(12):550.

24. Bray NL, Pimentel H, Melsted P, Pachter L. Near-optimal probabilistic RNA-seq quantification. Nat Biotechnol. 2016;34(5):525-7.

25. Pereira RO, Wende AR, Olsen C, Soto J, Rawlings T, Zhu Y, et al. Inducible overexpression of GLUT1 prevents mitochondrial dysfunction and attenuates structural remodeling in pressure overload but does not prevent left ventricular dysfunction. J Am Heart Assoc. 2013;2(5):e000301.

26. Mina AI, LeClair RA, LeClair KB, Cohen DE, Lantier L, Banks AS. CalR: A Web-Based Analysis Tool for Indirect Calorimetry Experiments. Cell Metab. 2018;28(4):656-66 e1.

27. Camporez JP, Asrih M, Zhang D, Kahn M, Samuel VT, Jurczak MJ, et al. Hepatic insulin resistance and increased hepatic glucose production in mice lacking Fgf21. J Endocrinol. 2015;226(3):207-17.

28. Deng J, Yuan F, Guo Y, Xiao Y, Niu Y, Deng Y, et al. Deletion of ATF4 in AgRP Neurons Promotes Fat Loss Mainly via Increasing Energy Expenditure. Diabetes. 2017;66(3):640-50.

29. Hernandez G, Luo T, Javed TA, Wen L, Kalwat MA, Vale K, et al. Pancreatitis is an FGF21-deficient state that is corrected by replacement therapy. Sci Transl Med. 2020;12(525).

30. Maruyama R, Shimizu M, Li J, Inoue J, Sato R. Fibroblast growth factor 21 induction by activating transcription factor 4 is regulated through three amino acid response elements in its promoter region. Biosci Biotechnol Biochem. 2016;80(5):929-34.

31. Ord T, Ord D, Ord T. TRIB3 limits FGF21 induction during in vitro and in vivo nutrient deficiencies by inhibiting C/EBP-ATF response elements in the Fgf21 promoter. Biochim Biophys Acta Gene Regul Mech. 2018;1861(3):271-81.

32. Klein Hazebroek M, Keipert S. Adapting to the Cold: A Role for Endogenous Fibroblast Growth Factor 21 in Thermoregulation? Front Endocrinol (Lausanne). 2020;11:389.

33. Hanssen MJ, Broeders E, Samms RJ, Vosselman MJ, van der Lans AA, Cheng CC, et al. Serum FGF21 levels are associated with brown adipose tissue activity in humans. Sci Rep. 2015;5:10275.

34. Keipert S, Kutschke M, Ost M, Schwarzmayr T, van Schothorst EM, Lamp D, et al. Long-Term Cold Adaptation Does Not Require FGF21 or UCP1. Cell Metab. 2017;26(2):437-46 e5.

35. Ameka M, Markan KR, Morgan DA, BonDurant LD, Idiga SO, Naber MC, et al. Liver Derived FGF21 Maintains Core Body Temperature During Acute Cold Exposure. Sci Rep. 2019;9(1):630.

36. Douris N, Stevanovic DM, Fisher FM, Cisu TI, Chee MJ, Nguyen NL, et al. Central Fibroblast Growth Factor 21 Browns White Fat via Sympathetic Action in Male Mice. Endocrinology. 2015;156(7):2470-81.

37. Cuevas-Ramos D, Mehta R, Aguilar-Salinas CA. Fibroblast Growth Factor 21 and Browning of White Adipose Tissue. Front Physiol. 2019;10:37.

38. Yoneshiro T, Wang Q, Tajima K, Matsushita M, Maki H, Igarashi K, et al. BCAA catabolism in brown fat controls energy homeostasis through SLC25A44. Nature. 2019;572(7771):614-9.

39. Allu PKR, Paulo E, Bertholet AM, Situ G, Lee SH, Wu Y, et al. Role of mTORC2 in biphasic regulation of brown fat metabolism in response to mild and severe cold. J Biol Chem. 2021;296:100632.

40. Labbe SM, Mouchiroud M, Caron A, Secco B, Freinkman E, Lamoureux G, et al. mTORC1 is Required for Brown Adipose Tissue Recruitment and Metabolic Adaptation to Cold. Sci Rep. 2016;6:37223.

41. Liu D, Bordicchia M, Zhang C, Fang H, Wei W, Li JL, et al. Activation of mTORC1 is essential for beta-adrenergic stimulation of adipose browning. J Clin Invest. 2016;126(5):1704-16.

42. Lee PL, Tang Y, Li H, Guertin DA. Raptor/mTORC1 loss in adipocytes causes progressive lipodystrophy and fatty liver disease. Mol Metab. 2016;5(6):422-32.

Figure Legends:

Figure 1: The integrated stress response is induced in BAT after cold exposure. A and B. Data collected in BAT of WT mice exposed to 30 °C or 4 °C for 3 days. **A.** Immunoblot of phosphorylated eIf2α normalized to total eIf2α and respective densitometric quantification. **B.** mRNA expression of the integrated stress response genes *Atf4*, *Fgf21* and *Gdf15.* **C-G.** Data collected in WT and ATF4 BAT KO mice at baseline conditions. **C.** Relative mRNA expression of *Atf4* in BAT normalized to *Gapdh.* **D.** Relative mRNA expression of *Atf4* in inguinal white adipose tissue (iWAT) normalized to *Gapdh.* **E.** Relative mRNA expression of *Fgf21* and *Gdf15* in BAT normalized to *Gapdh.* ISR (integrated stress response.) **F.** Serum FGF21 levels. **G.** Serum GDF15 levels. Data are expressed as means ± SEM. Significant differences were determined by Student's *t*-test, using a significance level of $P < 0.05$. * $p < 0.05$ significantly different vs. WT mice or 30 °C.

Figure 2: ATF4 BAT KO mice have reduced BAT mass and impaired glucose homeostasis at baseline conditions. A. Body mass. **B.** Total fat mass. **C.** Total lean mass. **D.** Brown adipose tissue (BAT) mass normalized to body mass. **E.** Gonadal white adipose tissue (gWAT) mass normalized to body mass. **F.** Inguinal white adipose tissue (iWAT) mass normalized to body mass. **G.** Energy expenditure. **H.** Locomotor activity. **I.** Food intake. **J.** Glucose tolerance test (GTT). **K.** Area under the curve for the GTT. **L.** Fasting glucose levels (after a 6-hr fast). **M.** Liver triglyceride levels. Data are expressed as means ± SEM. Significant differences were determined by Student's *t*-test, using a significance level of $P < 0.05$. * $p < 0.05$ significantly different vs. WT mice.

Figure 3: ATF4 expression in BAT is required for thermoregulation in mice. A-J. Data collected in WT and KO mice after 3 days of cold exposure (4 °C). **A.** Core body temperature **B.** Averaged core body temperature after 3 days at 4 °C. **C.** Relative mRNA expression of *Fgf21* in

BAT normalized to *Gapdh*. **D.** Serum FGF21 levels. **E.** BAT mass after 3 days of cold exposure normalized to body mass. **F.** mRNA expression of thermogenic genes in BAT normalized to *Gapdh*. **G.** Immunoblot of UCP1 in BAT normalized to GAPDH and its respective densitometric quantification. **H.** mRNA expression of *Atf4* in inguinal white adipose tissue (iWAT) normalized to *Gapdh*. **I.** mRNA expression of thermogenic genes in iWAT normalized to *Gapdh*. **J. K-P.** Data collected in WT and ATF4 BKO mice cold exposed for 4 hours following a 12-hr fast. **K.** Hourly core body temperature in ATF4 BKO mice. **L.** *Fgf21* mRNA levels in BAT of ATF4 BKO mice normalized to *Tbp.* **M.** FGF21 serum levels in ATF4 BKO mice. **N.** mRNA expression of thermogenic genes in BAT normalized to *Tbp*. **O.** Immunoblot of UCP1 in BAT normalized to β-actin and its respective densitometric quantification. **P.** mRNA expression of thermogenic genes in iWAT normalized to *Tbp*. Data are expressed as means ± SEM. Significant differences were determined by Student's *t*-test, using a significance level of $p < 0.05$. * $p < 0.05$; ** $p < 0.01$ significantly different vs. WT mice.

Figure 4: FGF21 BAT KO mice have normal body weight and glucose homeostasis at baseline conditions. A. Body mass. **B.** Total fat mass. **C.** Total lean mass. **D.** Food intake. **E.** Locomotor activity. **F.** Energy expenditure. **G.** Glucose tolerance test (GTT). **H.** Area under the curve for the GTT. **H.** Fasting glucose levels (after a 6-hr fast). Data are expressed as means ± SEM. Significant differences were determined by Student's *t*-test, using a significance level of $P < 0.05$. * Significantly different vs. WT mice.

Figure 5: FGF21 Expression in Thermogenic Adipocytes Is Dispensable for Thermoregulation. A. Averaged core body temperature after 3 days at 30 ˚C. **B-J.** Data collected in WT and KO mice after 3 days of cold exposure (4 ˚C). **B.** Averaged core body temperature after 3 days at 4 ˚C. **C.** Relative mRNA expression of *Fgf21* in BAT normalized to *Tbp*. **D.** Serum FGF21 levels. **E.** BAT mass after 3 days of cold exposure normalized to body

mass. **F.** mRNA expression of thermogenic genes in BAT normalized to *Tbp*. **G.** Immunoblot of UCP1 in BAT normalized to β-actin and its respective densitometric quantification. **H.** mRNA expression of *Fgf21* in inguinal white adipose tissue (iWAT) normalized to *Tbp*. **I.** mRNA expression of thermogenic genes in iWAT normalized to *Tbp*. **J.** Immunoblot of UCP1 in iWAT normalized to β-actin and its respective densitometric quantification. **K-P.** Data collected in WT and FGF21 BKO mice cold exposed for 4 hours following a 12-hr fast. **K.** Hourly core body temperature. **L.** *Fgf21* mRNA levels in normalized to *Tbp.* **M.** FGF21 serum levels. **N.** mRNA expression of thermogenic genes in BAT normalized to *Tbp*. **O.** Immunoblot of UCP1 in BAT normalized to β-actin and its respective densitometric quantification. **P.** mRNA expression of thermogenic genes in iWAT normalized to *Tbp*. Data are expressed as means ± SEM. Significant differences were determined by Student's *t*-test, using a significance level of $p < 0.05$. * $p < 0.05$ significantly different vs. WT mice

Figure 6: Transcriptome Analysis Reveals Downregulation of Genes Involved in Amino Acid Metabolism in ATF4 BKO Mice. A-B. Data collected from brown adipose tissue (BAT) of WT and ATF4 BKO mice cold exposed for 3 days (Differential gene expression and Ingenuity Pathway Analysis). **A.** Heatmap of differentially expressed genes annotated in the IPA database as ATF4 targets. Plotted are log2(x+1) transformed counts scaled by row. **B.** Genes differentially expressed have a significant overlap (adjusted p-value ≤ 0.05) with genes that are annotated to be involved in various diseases or have common biological functions that regulate genes with a significant overlap (adjusted p-value ≤ 0.05) to those differentially expressed in ATF4KO BAT. The number of genes in the data set annotated as being involved in the disease or have a particular biological function is plotted on the x-axis. Bubble size = -log (adjusted p-value) and color = z-score; indicates the potential impact of the differential gene expression pattern on the disease or biological function. **C.** Relative mRNA expression of amino acid

transporter and metabolism genes in BAT of ATF4 BKO mice normalized to *Tbp* expression. **D.** Immunoblot of phosphorylated S6 in BAT normalized to total S6 and its respective densitometric quantification. Data are expressed as means ± SEM. Significant differences were determined by Student's *t*-test, using a significance level of $p<0.05$. * $p < 0.05$; ** $p < 0.01$; *** $p < 0.001$; **** $p < 0.001$ significantly different vs. WT mice.

Figure 1

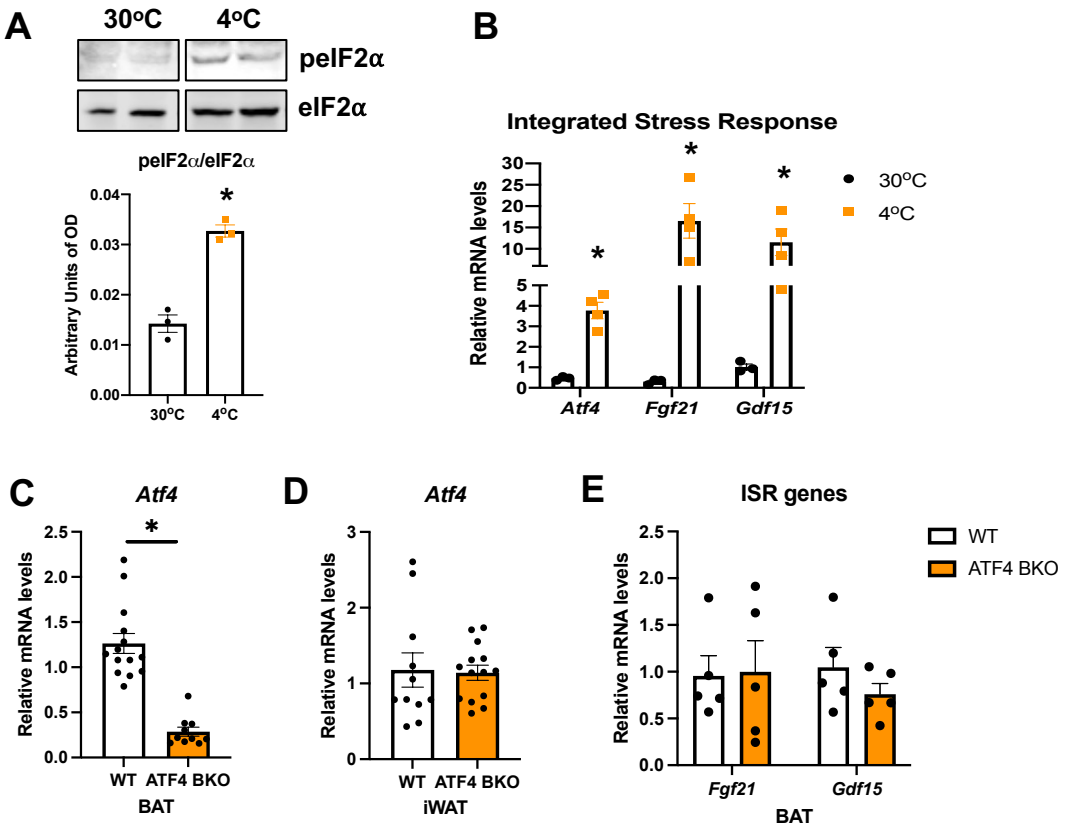
A
30°C
4°C
peIF2α
eIF2α
peIF2α/eIF2α
Arbitrary Units of OD
0.04
0.03
0.02
0.01
0.00
30°C
4°C
B
Integrated Stress Response
Relative mRNA levels
30°C
4°C
Atf4
Fgf21
Gdf15
C
Atf4
Relative mRNA levels
WT
ATF4 BKO
BAT
D
Atf4
Relative mRNA levels
WT
ATF4 BKO
iWAT
E
ISR genes
Relative mRNA levels
WT
ATF4 BKO
Fgf21
Gdf15
BAT
F
Serum FGF21
pg/ml
WT
KO
G
Serum GDF15
pg/ml
WT
KO

Figure 2

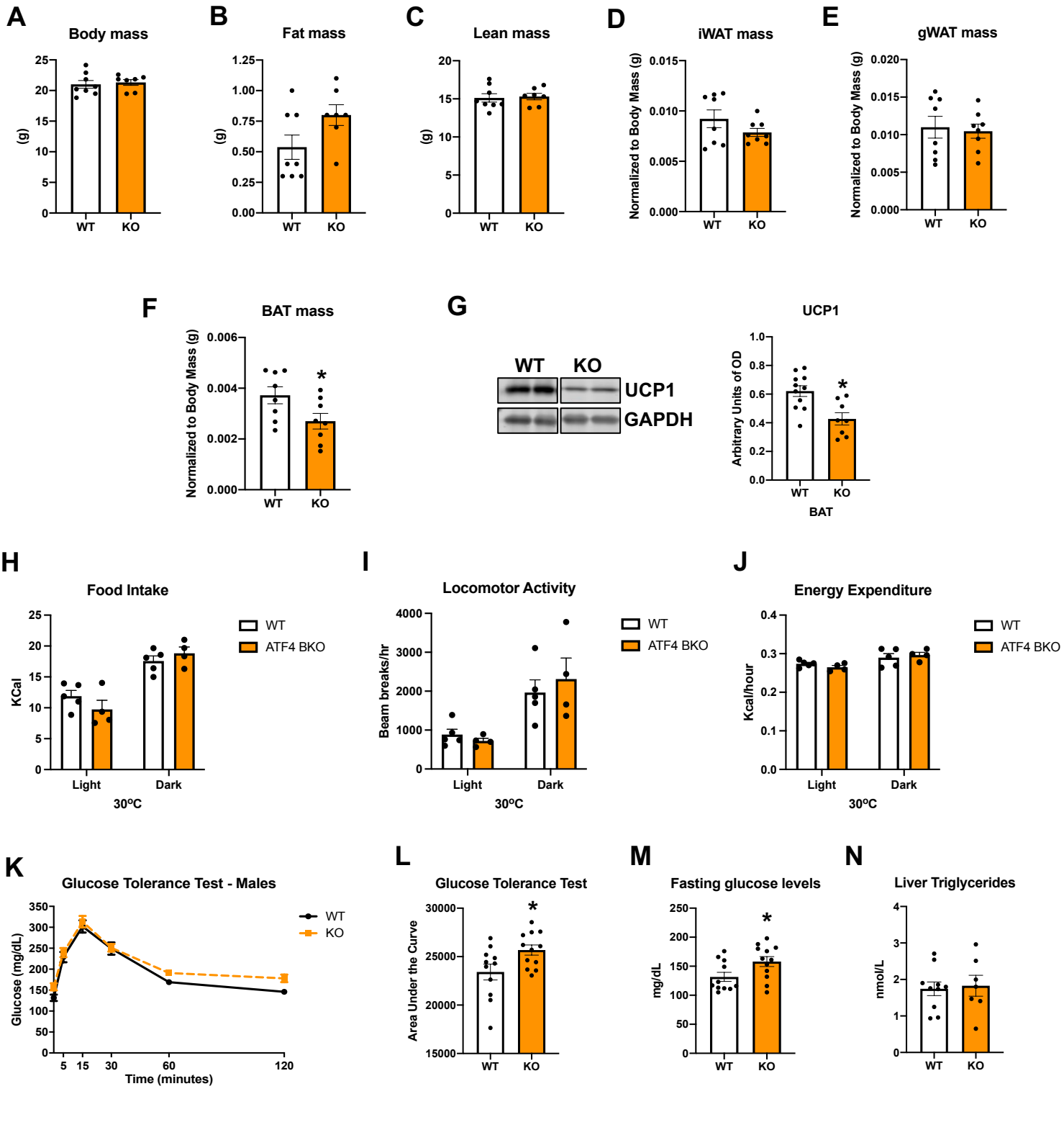
A
Body mass
(g)
WT
KO
B
Fat mass
(g)
C
Lean mass
(g)
D
iWAT mass
Normalized to Body Mass (g)
E
gWAT mass
Normalized to Body Mass (g)
F
BAT mass
Normalized to Body Mass (g)
*
G
WT
KO
UCP1
GAPDH
UCP1
Arbitrary Units of OD
BAT
H
Food Intake
KCal
WT
ATF4 BKO
Light
Dark
30ºC
I
Locomotor Activity
Beam breaks/hr
J
Energy Expenditure
Kcal/hour
K
Glucose Tolerance Test - Males
Glucose (mg/dL)
Time (minutes)
L
Glucose Tolerance Test
Area Under the Curve
M
Fasting glucose levels
mg/dL
N
Liver Triglycerides
nmol/L

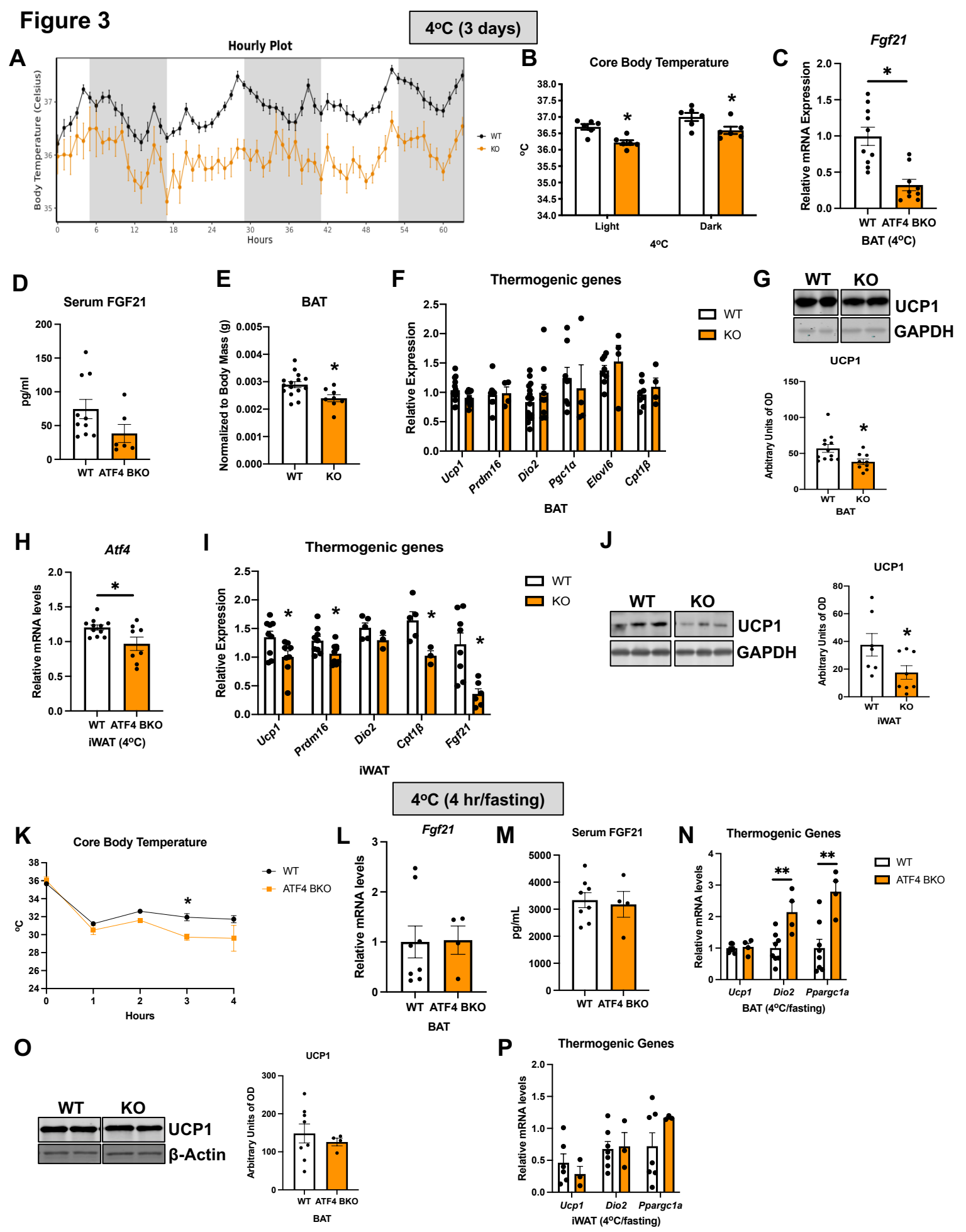
Figure 3
4ºC (3 days)
A
Hourly Plot
Body Temperature (Celsius)
Hours
WT
KO
B
Core Body Temperature
ºC
Light
Dark
4ºC
C
Fgf21
Relative mRNA Expression
WT ATF4 BKO
BAT (4ºC)
D
Serum FGF21
pg/ml
WT ATF4 BKO
E
BAT
Normalized to Body Mass (g)
WT
KO
F
Thermogenic genes
Relative Expression
Ucp1
Prdm16
Dio2
Pgc1α
Elovl6
Cpt1β
BAT
G
WT
KO
UCP1
GAPDH
UCP1
Arbitrary Units of OD
BAT
H
Atf4
Relative mRNA levels
WT ATF4 BKO
iWAT (4ºC)
I
Thermogenic genes
Relative Expression
Ucp1
Prdm16
Dio2
Cpt1β
Fgf21
iWAT
J
WT
KO
UCP1
GAPDH
UCP1
Arbitrary Units of OD
iWAT
4ºC (4 hr/fasting)
K
Core Body Temperature
ºC
Hours
WT
ATF4 BKO
L
Fgf21
Relative mRNA levels
WT ATF4 BKO
BAT
M
Serum FGF21
pg/mL
WT ATF4 BKO
N
Thermogenic Genes
Relative mRNA levels
Ucp1
Dio2
Ppargc1a
BAT (4ºC/fasting)
WT
ATF4 BKO
O
WT
KO
UCP1
β-Actin
UCP1
Arbitrary Units of OD
WT ATF4 BKO
BAT
P
Thermogenic Genes
Relative mRNA levels
Ucp1
Dio2
Ppargc1a
iWAT (4ºC/fasting)

Figure 4

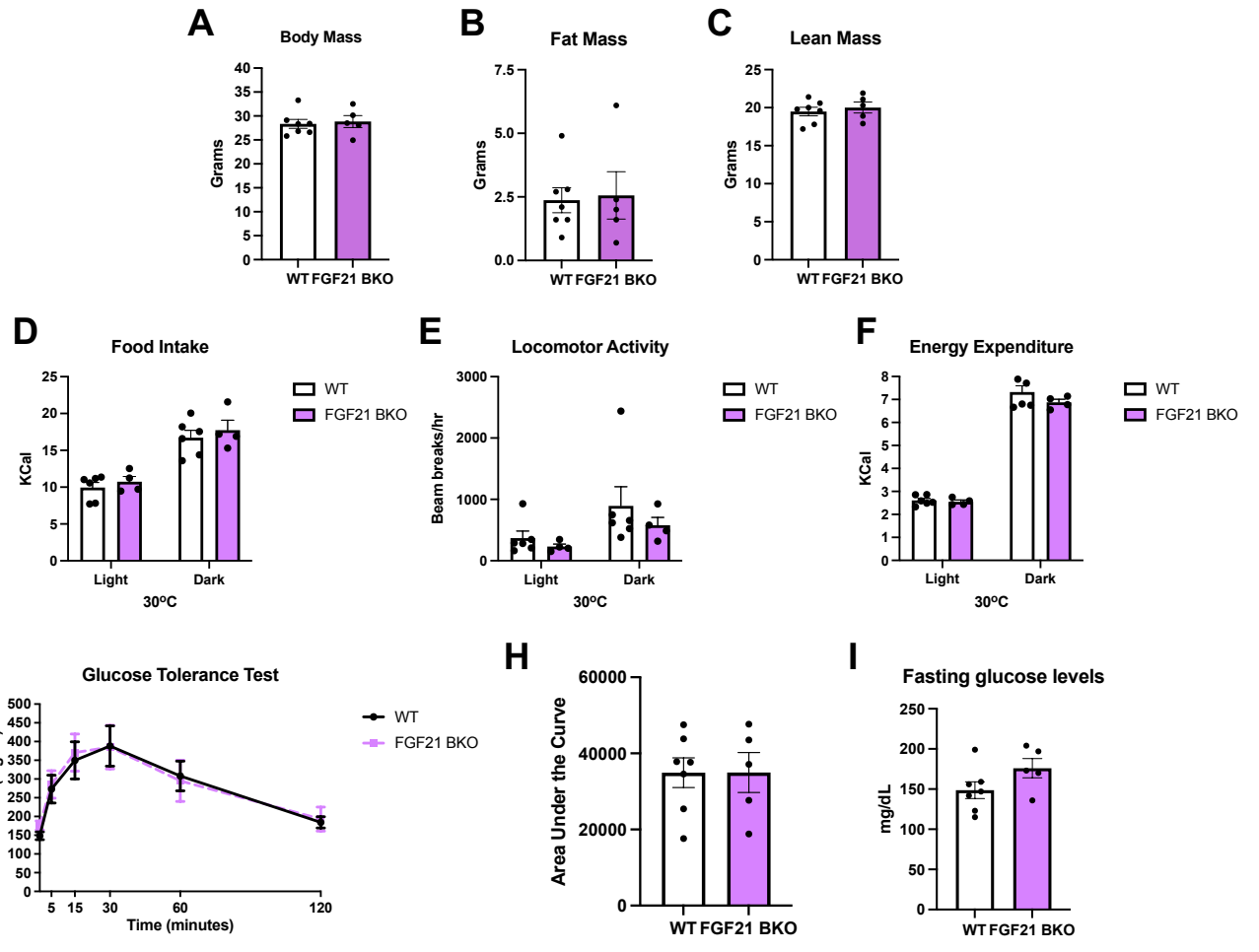
A
Body Mass
Grams
WT FGF21 BKO
B
Fat Mass
Grams
WT FGF21 BKO
C
Lean Mass
Grams
WT FGF21 BKO
D
Food Intake
KCal
Light
Dark
30°C
WT
FGF21 BKO
E
Locomotor Activity
Beam breaks/hr
Light
Dark
30°C
WT
FGF21 BKO
F
Energy Expenditure
KCal
Light
Dark
30°C
WT
FGF21 BKO
G
Glucose Tolerance Test
Glucose (mg/dL)
Time (minutes)
WT
FGF21 BKO
H
Area Under the Curve
WT FGF21 BKO
I
Fasting glucose levels
mg/dL
WT FGF21 BKO

Figure 5

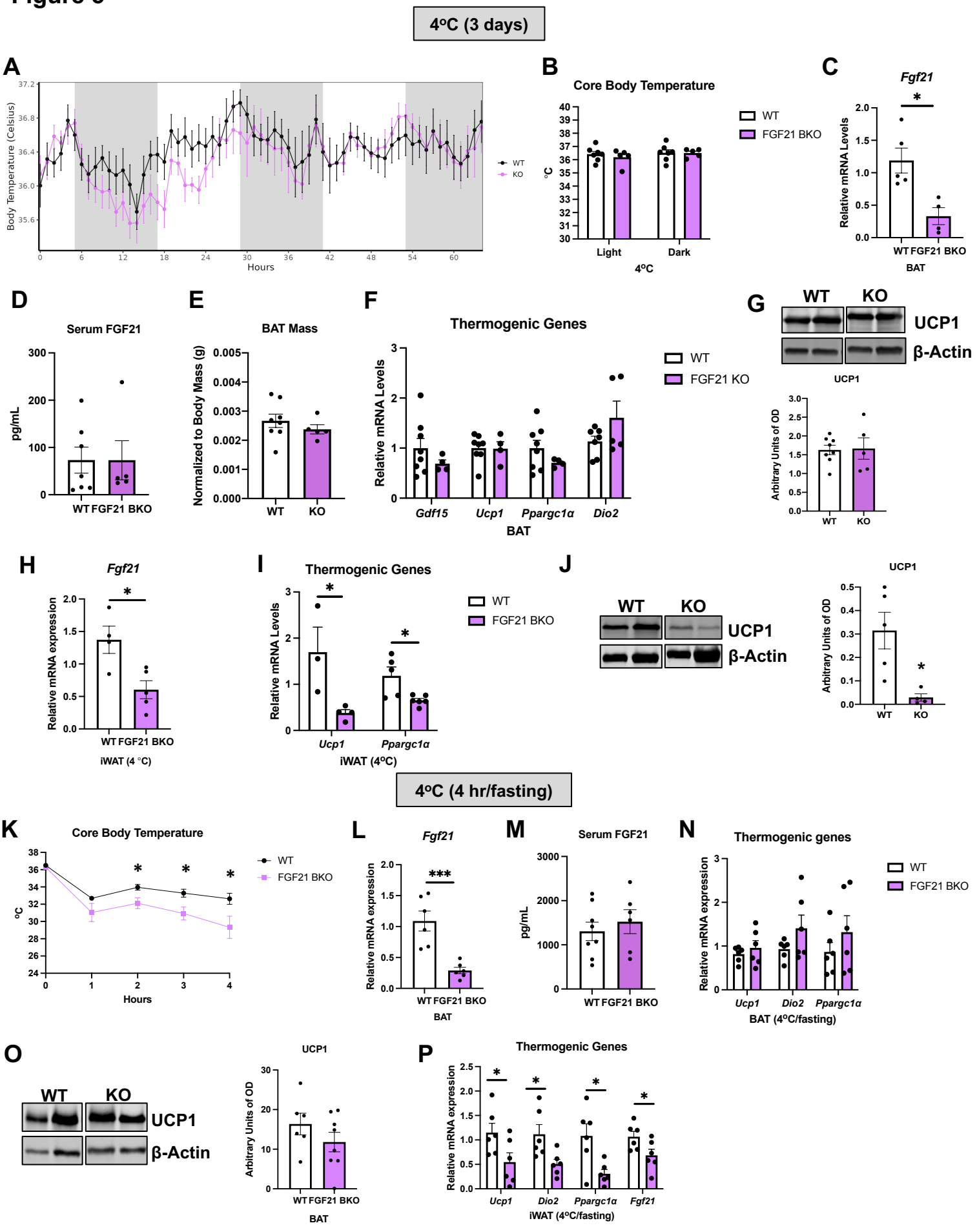
4ºC (3 days)
A
Body Temperature (Celsius)
Hours
WT
KO
B
Core Body Temperature
°C
Light
Dark
4ºC
WT
FGF21 BKO
C
Fgf21
Relative mRNA Levels
WT FGF21 BKO
BAT
D
Serum FGF21
pg/mL
WT FGF21 BKO
E
BAT Mass
Normalized to Body Mass (g)
WT
KO
F
Thermogenic Genes
Relative mRNA Levels
Gdf15
Ucp1
Ppargc1α
Dio2
BAT
WT
FGF21 KO
G
WT
KO
UCP1
β-Actin
UCP1
Arbitrary Units of OD
WT
KO
H
Fgf21
Relative mRNA expression
WT FGF21 BKO
iWAT (4 °C)
I
Thermogenic Genes
Relative mRNA Levels
Ucp1
Ppargc1α
iWAT (4ºC)
WT
FGF21 BKO
J
WT
KO
UCP1
β-Actin
UCP1
Arbitrary Units of OD
WT
KO
4ºC (4 hr/fasting)
K
Core Body Temperature
°C
Hours
WT
FGF21 BKO
L
Fgf21
Relative mRNA expression
WT FGF21 BKO
BAT
M
Serum FGF21
pg/mL
WT FGF21 BKO
N
Thermogenic genes
Relative mRNA expression
Ucp1
Dio2
Ppargc1α
BAT (4ºC/fasting)
WT
FGF21 BKO
O
WT
KO
UCP1
β-Actin
UCP1
Arbitrary Units of OD
WT FGF21 BKO
BAT
P
Thermogenic Genes
Relative mRNA expression
Ucp1
Dio2
Ppargc1α
Fgf21
iWAT (4ºC/fasting)

Figure 6

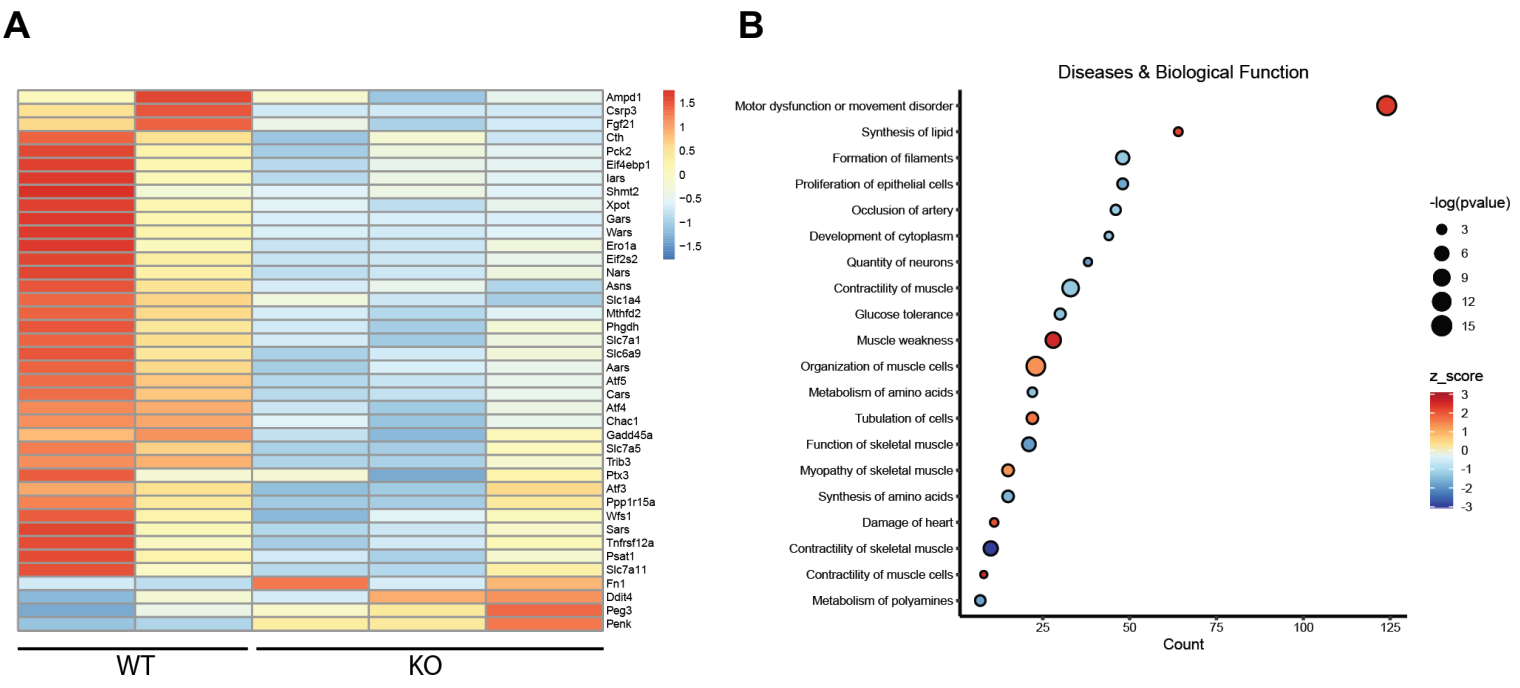
A
Ampd1
Csrp3
Fgf21
Cth
Pck2
Eif4ebp1
Iars
Shmt2
Xpot
Gars
Wars
Ero1a
Eif2s2
Nars
Asns
Slc1a4
Mthfd2
Phgdh
Slc7a1
Slc6a9
Aars
Atf5
Cars
Atf4
Chac1
Gadd45a
Slc7a5
Trib3
Ptx3
Atf3
Ppp1r15a
Wfs1
Sars
Tnfrsf12a
Psat1
Slc7a11
Fn1
Ddit4
Peg3
Penk
1.5
1
0.5
0
−0.5
−1
−1.5
WT
KO
B
Diseases & Biological Function
Motor dysfunction or movement disorder
Synthesis of lipid
Formation of filaments
Proliferation of epithelial cells
Occlusion of artery
Development of cytoplasm
Quantity of neurons
Contractility of muscle
Glucose tolerance
Muscle weakness
Organization of muscle cells
Metabolism of amino acids
Tubulation of cells
Function of skeletal muscle
Myopathy of skeletal muscle
Synthesis of amino acids
Damage of heart
Contractility of skeletal muscle
Contractility of muscle cells
Metabolism of polyamines
25
50
75
100
125
Count
-log(pvalue)
3
6
9
12
15
z_score
3
2
1
0
-1
-2
-3

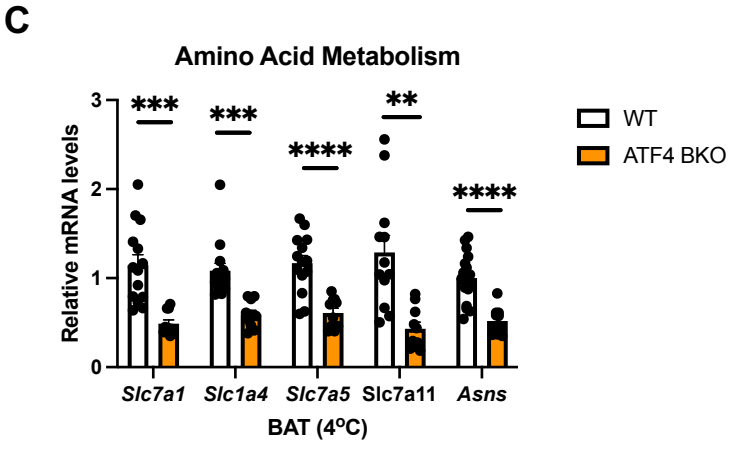
C
Amino Acid Metabolism
Relative mRNA levels
3
2
1
0
***
***
****
**
****
Slc7a1
Slc1a4
Slc7a5
Slc7a11
Asns
BAT (4°C)
WT
ATF4 BKO

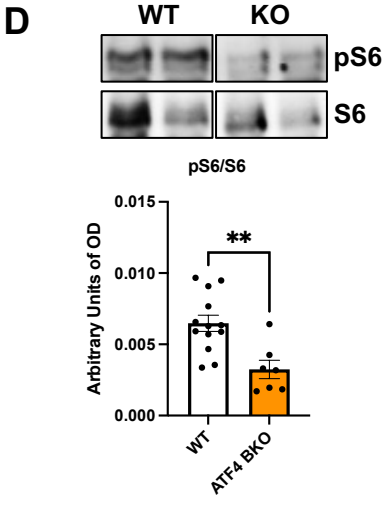
D
WT
KO
pS6
S6
pS6/S6
0.015
0.010
0.005
0.000
**
Arbitrary Units of OD
WT
ATF4 BKO